

Tracking intracellular dynamics through extracellular measurements

Franz Hamilton^{1*}, Tyrus Berry², Timothy Sauer²

1 North Carolina State University, Department of Mathematics, Raleigh, 27695, USA
2 George Mason University, Department of Mathematical Sciences, Fairfax, 22030, USA

* fwhamilt@ncsu.edu

Abstract

Extracellular recordings of neuronal cells are frequently a part of *in vitro* and *in vivo* experimental studies as a means of monitoring network-level dynamics. Their connections to intracellular dynamics are not well understood. Single-unit recordings are a more direct way to measure intracellular dynamics, but are typically difficult and expensive. On the other hand, simple differential equations models exist for single neurons. In this article, we apply a recent advance in data assimilation theory, designed to correct bias in general observation functions, toward the reconstruction of model-based intracellular dynamics from extracellular recordings.

Author summary

Model-based inference of experimental variables is predicated on a known relationship between the model dynamics and the data collected from the experimental system. If this relationship is not known, or known with error, the resulting inference of the system variables is prone to inaccuracies. This problem is exemplified in neuroscience studies where experimental recordings of extracellular, or outside the cell, activity may be used to infer intracellular, or inside the cell, dynamics. In this article, we demonstrate the use of a novel method for reconciling this error towards the goal of tracking intracellular neuronal dynamics using extracellular measurements.

Introduction

In vitro and *in vivo* neuronal experiments in the laboratory are frequently centered around measurements of cell potential. While intracellular (within cell) recordings give precise, single-cell measurements of neuronal potential, they are difficult, often obtained under nonphysiological conditions, and typically do not allow for multi-site recordings. Extracellular recordings are easier to obtain, but the relation to intracellular dynamics is complicated. In particular, the morphology of the spikes and other aspects of the recordings are usually quite different. A common hypothesis is that the extracellular potential of a neuronal cell is roughly approximated by the negative time derivative of the intracellular potential. However, simultaneous intracellular and extracellular measurements have shown that this relationship does not hold throughout the entire evolution of a spike [1]. Fig. 1 shows an example time series [2] comparing intracellular and extracellular recordings (see [1, 3] for more details on the experimental design and

study). This representative example demonstrates some of the differences between the two types of cell measurements.

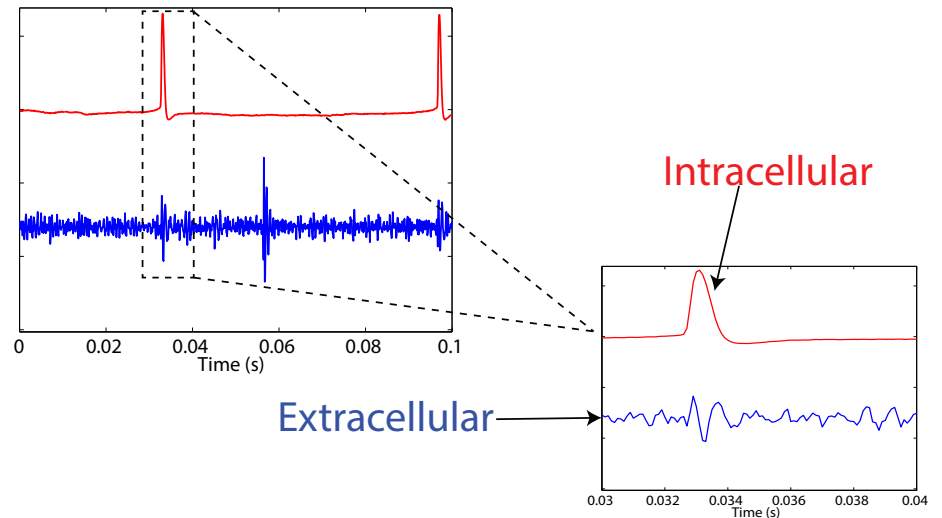


Fig 1. Example of simultaneous intracellular and extracellular recordings from a neuronal experiment in the laboratory. Data from [1–3]. Intracellular recordings (red trace) occur inside an individual cell, whereas extracellular recordings (blue trace) occur outside the cell and often result in the recording of activity from several different cells. While neuronal models describe the intracellular cell dynamics, experimental recordings often consist of extracellular measurements, particularly when examining network-level dynamics. There is a fundamental difference between the recorded potentials, for example the biphasic waveform of the extracellular recording compared to the monophasic waveform of the intracellular recording.

Modern methods of data assimilation are adept at reconstructing hidden variables, as long as details of their relations to observations are known. If we consider the intracellular dynamics as the hidden variable, it is the lack of an explicit “observation function” that has limited the applicability of these methods. While ad hoc methods for pre-processing the extracellular measurements have been used (see for example [4, 5]), these approaches suffer from never learning the true mapping from the intracellular state to the extracellular observation space.

In this article we assume as given an extracellular recording and a model of single-cell neuronal dynamics. We will exploit a recent advance [6] in data assimilation to fit the recording to the individual cell dynamics, in absence of a known relation between them. The recent advance shows how to learn state-dependent observation function bias while filtering a signal. The approach is general enough to be used with a wide range of data assimilation methods, including nonlinear methods such as the ensemble Kalman filter. The main point is that even though the exact observation function of the single-cell dynamics that relates its activity to the extracellular recording is unknown, the connection can be gradually learned from an iterative processing of the data.

We demonstrate this methodology on several neuro-inspired examples, specifically extending application of the method developed in [6] to situations of severe model error. We assume that we have a generic neuron model, namely the Fitzhugh-Nagumo system, and use it to reconstruct the intracellular dynamics of observed extracellular time series. We begin, as proof of concept, by showing the successful reconstruction of the intracellular state given extracellular observations of a stochastic Fitzhugh-Nagumo cell.

To further simulate the model error we will encounter when analyzing experimental data, we consider the assimilation of extracellular data from a more sophisticated model, the Hodgkin-Huxley system. Finally, we demonstrate the utility of our method in recovering the intracellular dynamics in an experimental setting by assimilating *in vivo* extracellular recordings.

Methods

The filtering problem

In the general filtering problem, we assume a system with n -dimensional state vector x and m -dimensional observation vector y defined by

$$\begin{aligned} x_k &= f(x_{k-1}) + w_{k-1} \\ y_k &= h(x_k) + v_k \end{aligned} \tag{1}$$

where w_{k-1} and v_k are white noise processes with covariance matrices Q and R , respectively. f represents the system dynamics and h is an observation function that maps the model state to the observation space. The goal is to sequentially estimate the state of the system given some noisy observations.

In the case of linear system dynamics and linear observation function, the Kalman filter [7] gives the optimal estimate of the system state. Extensions of the Kalman filter to nonlinear situations include the extended Kalman filter and ensemble-based Kalman filters [8–18], which approximate nonlinear systems and gives near-optimal estimates. In either linear or nonlinear situation, the assumption is that both f and h are known, allowing the filter to alternate between a forecast and analysis step. During the filter’s forecast, a model-based prediction of the system state and covariance is made. The predicted state is then mapped to observation space through known observation function h , giving a model-predicted observation. These state and covariance predictions are updated in the analysis step, which relies on the difference between the actual observation and the model predicted observation. This procedure continues iteratively for each observation.

Without loss of generality, here we consider use of the ensemble Kalman filter (EnKF) for nonlinear state estimation. The EnKF approximates a nonlinear system by forming an ensemble, such as through the unscented transformation (see for example [8]). At the k th step of the filter there is an estimate of the state x_{k-1}^+ and the covariance matrix P_{k-1}^+ . In the unscented version of the EnKF, the singular value decomposition is used to find the symmetric positive definite square root S_{k-1}^+ of the matrix P_{k-1}^+ , allowing us to form an ensemble of E state vectors where the i^{th} ensemble member is denoted $x_{i,k-1}^+$.

The model f is applied to the ensemble, and then observed with function h

$$\begin{aligned} x_{i,k}^- &= f\left(x_{i,k-1}^+\right) \\ y_{i,k}^- &= h\left(x_{i,k}^-\right) \end{aligned} \tag{3}$$

The mean of the resulting state and observed ensembles gives the prior state estimate x_k^- and predicted observation y_k^- , respectively. Denoting the covariance matrices P_k^- and P_k^y of the resulting state and observed ensemble, and the cross-covariance matrix

P_k^{xy} , we define

$$\begin{aligned}
 P_k^- &= \frac{1}{E} \sum_{i=1}^E (x_{i,k}^- - x_k^-) (x_{i,k}^- - x_k^-)^T + Q \\
 P_k^y &= \frac{1}{E} \sum_{i=1}^E (y_{i,k}^- - y_k^-) (y_{i,k}^- - y_k^-)^T + R \\
 P_k^{xy} &= \frac{1}{E} \sum_{i=1}^E (x_{i,k}^- - x_k^-) (y_{i,k}^- - y_k^-)^T
 \end{aligned} \tag{4}$$

and use the equations

$$\begin{aligned}
 K_k &= P_k^{xy} (P_k^y)^{-1} \\
 P_k^+ &= P_k^- - K_k P_k^{yx} \\
 x_k^+ &= x_k^- + K_k (y_k - y_k^-).
 \end{aligned} \tag{5}$$

to update the state and covariance estimates with the observation y_k . Q and R are generally unknown quantities that have to be estimated. We use the method of [19] for the adaptive estimation of these noise covariance matrices.

Filtering with an unknown observation function

The update of the state and covariance predictions in the analysis step is dependent on the correct observation function h being known. Of course in many applications, such as in the mapping of intracellular model state to extracellular observation space, this function is known imperfectly and in its place an incorrect function g is used. We will assume the true dynamics are represented by Eq. 1 and Eq. 2, but that the filter is supplied with Eq. 1 and

$$y_k = g(x_k) + v_k. \tag{6}$$

Define $b(x_k) = h(x_k) - g(x_k)$ to be the state-dependent *bias* in the observation resulting from use of the incorrect observation function. Recent work [20] addressed the issue of error caused by an unknown observation function by using a training set consisting of observations and the corresponding true state with which to build an estimate of the bias. Here, we assume that no training data of the true state are available and implement a recent advance [6] in data assimilation that attempts to empirically estimate the bias. We present a summary of the technique here, further details of which can be found in [6].

The general idea is to iteratively update the incorrect observation function g by obtaining improved estimates of the bias. We begin with an initial estimate of the bias function $b^{(0)} = 0$, and set $g^{(0)} = g + b^{(0)} = g$. The filter is given the known system dynamics f , the initial incorrect observation function $g^{(0)}$, and the observations y , and provides an estimate of the state at each observation time k , which we denote $x_k^{(0)}$. This initial state estimate will be subject to large errors, due to the unaccounted-for bias. Using this imperfect state estimate, we calculate a noisy estimate of the bias, $\hat{b}_k^{(0)}$, corresponding to observation y_k where

$$\hat{b}_k^{(0)} = y_k - g(x_k^{(0)}). \tag{7}$$

Due to noise in the data as well as the imperfection of the state estimate, $\hat{b}_k^{(0)}$ will not accurately reflect the true bias, $b(x_k)$. To build a better estimate of $b(x_k)$, we use

Takens' method of attractor reconstruction [21–24] to reconstruct the bias function. 105
 Given observation y_k , consider delay-coordinate vector $z_k = [y_k, y_{k-1}, \dots, y_{k-d}]$ where d 106
 is the number of delays. Delay vector z_k represents the state of the system [21, 23]. To 107
 build the reconstruction, we locate the N nearest neighbors (with respect to Euclidean 108
 distance) z_{i_1}, \dots, z_{i_N} , where 109

$$z_{i_j} = [y_{i_j}, y_{i_j-1}, \dots, y_{i_j-d}]$$

within the set of observations. Once the neighbors are found, the corresponding 110
 $\hat{b}_{i_1}^{(0)}, \hat{b}_{i_2}^{(0)}, \dots, \hat{b}_{i_N}^{(0)}$ values are used in a locally constant model to estimate $b(x_k)$ 111

$$b^{(0)}(x_k) = w_{i_1} \hat{b}_{i_1}^{(0)} + w_{i_2} \hat{b}_{i_2}^{(0)} + \dots + w_{i_N} \hat{b}_{i_N}^{(0)}. \quad (8)$$

where the weight for j^{th} neighbor is defined as 112

$$w_{i_j} = \frac{e^{-(d_{i_j}/\sigma)}}{\sum_{j=1}^N e^{-(d_{i_j}/\sigma)}}.$$

Here, d_{i_j} is the distance of z_{i_j} to the current delay-coordinate vector and σ is the 113
 bandwidth which controls the contribution of each neighbor in the local model. We set 114
 σ to be half of the mean distance of the neighbors. 115

Note that Eq. 8 is still just an approximation of $b(x_k)$, although a more accurate 116
 estimate compared to Eq. 7. The observation function can now be updated as 117

$$g^{(1)} = g + b^{(0)}.$$

This improved observation function is given to the filter, and the data are re-processed. 118
 An improved state estimate, $x_k^{(1)}$, at time k is obtained, a more accurate reconstruction, 119
 $b^{(1)}(x_k)$, of the bias is formed using Eqs. 7-8 and the observation function is updated, 120
 $g^{(2)} = g + b^{(1)}$. 121

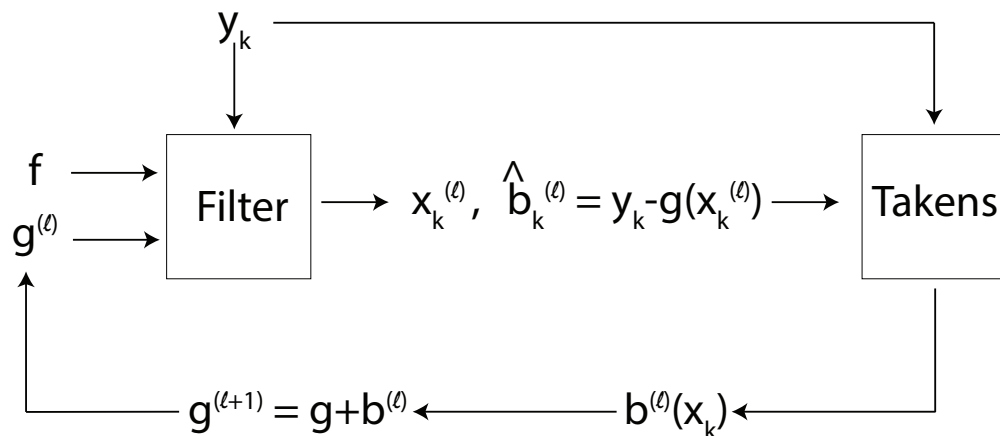


Fig 2. Schematic of algorithm for correcting observation error.

The method continues iteratively, each iteration an improved reconstruction of $b(x_k)$ 122
 is obtained resulting in a better estimate of the state on the next iteration. To 123
 summarize the method for $\ell = 0, 1, \dots, M$ iterations 124

1. Initialize $g^{(0)} = g$ and $b^{(0)} = 0$ 125

2. For each observation y_k , use filter to estimate state $x_k^{(\ell)}$ given known f and observation function $g^{(\ell)}$ 126
127
3. Calculate noisy bias estimate $\hat{b}_k^{(\ell)} = y_k - g(x_k^{(\ell)})$ 128
4. Use Takens' method to reconstruct estimate of bias function, $b^{(\ell)}(x_k)$ 129
5. Update observation function, $g^{(\ell+1)} = g + b^{(\ell)}$ 130
6. Repeat steps 2-5 until convergence 131

We determine that our method has converged when the change between successive reconstructions of the bias functions falls below some threshold. Figure 2 shows a schematic view of the steps of the algorithm. 132
133
134

Results 135

In the results presented below, we assume noisy extracellular data are available from a neuronal system and we implement an EnKF with a generic intracellular spiking model to reconstruct the intracellular state of the system. Specifically, our EnKF is provided the Fitzhugh-Nagumo model [25,26]

$$\begin{aligned} \dot{v} &= -w + v - \frac{v^3}{3} + I \\ \dot{w} &= \frac{v + 0.7 - 0.8w}{\tau} \end{aligned} \tag{9}$$

where I is a known stimulating current and τ is a time-scale parameter that is used to adjust the spiking frequency of the model to that of the data. The variable v represents the intracellular potential and w is a recovery variable that lumps together the effects of different ionic currents. 136
137
138
139

Motivated by experimental scenarios, we will rely on the ansatz that measurements of the neuron extracellular potential are given by the negative time derivative of the intracellular potential. Thus give the EnKF is provided a “best guess”, though likely incorrect, observation function g

$$g(v, w) = - \left(-w + v - \frac{v^3}{3} + I \right) \tag{10}$$

which is just the negative right-hand side of the \dot{v} differential equation in Eq. 9. 140

Throughout, we will compare our bias corrected filter with the standard filter (essentially, the $\ell = 0$ iteration of our method) which assumes no bias correction. Due to the extreme error caused by the biased observations, we limit the diagonal of the estimated noise covariances matrices to prevent overfitting or underfitting of the data. 141
142
143
144

State estimation with an incorrect observation function 145

We consider the noise-driven Fitzhugh-Nagumo system

$$\begin{aligned} \dot{v} &= -w + v - \frac{v^3}{3} + I + I_{\text{noise}} \\ \dot{w} &= \frac{v + 0.7 - 0.8w}{12.5} \end{aligned} \tag{11}$$

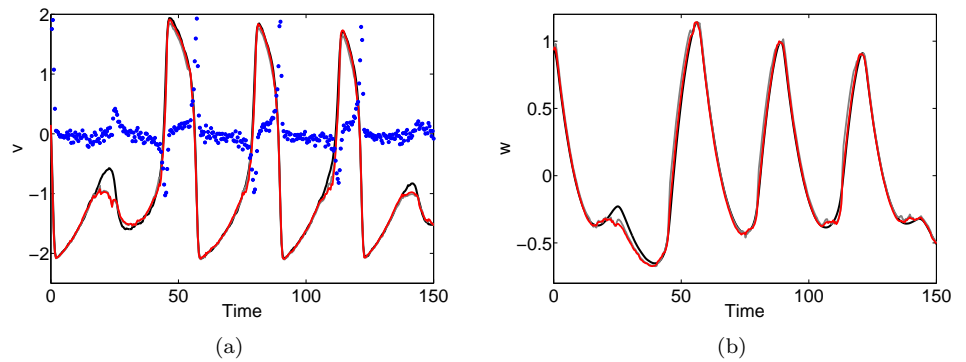


Fig 3. Results from reconstructing the state of a noise driven Fitzhugh-Nagumo system with small observation function error. True observation function $h(v, w) = 0.1f_1^2(v, w) - 0.9f_1(v, w) + 0.01$ is unknown. Given the observations (blue circles), we attempt to reconstruct the intracellular potential, v , and lump ionic recovery variable, w (solid black lines). In this example, the error between the filter observation function and true observation function is small enough that the standard filter (solid gray line) is able to provide accurate estimates of the variable trajectories (RMSE = 0.10, 0.07 for v and w respectively). The bias-corrected filter provides small, but not substantial improvements (RMSE = 0.10, 0.03 for v and w respectively)

where $I = 0.3 \sin\left(\frac{2\pi}{30}t\right) + 0.1$ is a periodic forcing current and I_{noise} is a mean 0 Gaussian noise current with variance $\sigma^2 = 0.005$. We assume that 2400 seconds of data are available, sampled at rate $dt = 0.4$. The true observation function

$$h(v, w) = \alpha_1 f_1^2(v, w) + \alpha_2 f_1(v, w) + \alpha_3,$$

where $f_1(v, w) = -w + v - \frac{v^3}{3} + I + I_{noise}$, is unknown and in its place we give the EnKF the observation function in Eq. 10. Note that there is a degree of model error in this example since Eq. 11 is stochastically driven whereas our assimilation model described by Eq. 9 does not account for this additional noise term.

In our first example, consider a situation where there is a small discrepancy between the true observation function h and our filter observation function g . Namely, our observations of Eq. 11 are given by

$$h(v, w) = 0.1f_1^2(v, w) - 0.9f_1(v, w) + 0.01. \tag{12}$$

Fig. 3 shows the results of reconstructing v and w (black solid lines) given the observations (blue circles) resulting from the function in Eq. 12. The solid gray line denotes the EnKF estimate without bias correction and the solid red line the estimate with bias correction. Note that the bias in this example is small, and as such the standard EnKF is able to handle the error and give good estimates of the system state by adjusting the Q and R covariance matrices (RMSE = 0.10, 0.07 for v and w respectively). The bias corrected filter, which uses $d = 5$ delays and $N = 20$ nearest neighbors to reconstruct the bias function, gives a slight improvement on the reconstruction of w , but in general performs comparably to the standard filter (RMSE = 0.10, 0.03 for v and w respectively). This result is not surprising, as we would not expect our bias-corrected filter to have much of an affect when the observational bias is low.

When the error in the observation function increases, the standard filter fails to accurately reconstruct the system dynamics. As an example, consider a large

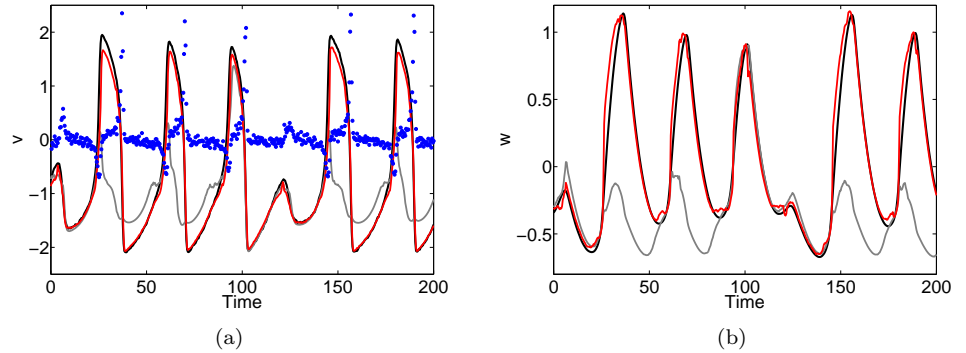


Fig 4. Results from reconstructing the state of a noise driven Fitzhugh-Nagumo system with large observation function error. Blue circles denote system observation. The large error between the filter observation function and the unknown true observation function, $h(v, w) = 0.25f_1^2(v, w) - 0.85f_1(v, w) + 0.02$, causes the standard filter (solid gray line) to fail in tracking the system dynamics (RMSE = 0.95, 0.53 for v and w respectively). The bias-corrected filter significantly improves on the state reconstruction (RMSE = 0.26, 0.12 for v and w respectively)

observation error scenario where the true observation function is given by

$$h(v, w) = 0.25f_1^2(v, w) - 0.85f_1(v, w) + 0.02. \quad (13)$$

Fig. 4 shows the results of reconstructing the system state in this large bias situation. The filter with no bias correction (solid gray line) fails to track the dynamics of the variables (RMSE = 0.95, 0.53 for v and w respectively) while the bias-corrected filter (solid red line) is able to accurately reconstruct the system dynamics (RMSE = 0.26, 0.12 for v and w respectively). This significant improvement in state reconstruction highlights the capability of our method for reconciling large errors caused by observational mismatch.

Reconstructing intracellular potential from extracellular measurements

The next example explores the assimilation of data from a Hodgkin-Huxley cell to a Fitzhugh-Nagumo model. The Hodgkin-Huxley system [27] is a detailed neuron model defined by

$$\begin{aligned} C\dot{V} &= -g_1m^3h(V - E_1) - g_2n^4(V - E_2) - g_3(V - E_3) + 7 + I_{\text{noise}} \\ \dot{m} &= (1 - m)\alpha_m(V - E_0) - m\beta_m(V - E_0) \\ \dot{n} &= (1 - n)\alpha_n(V - E_0) - n\beta_n(V - E_0) \\ \dot{h} &= (1 - h)\alpha_h(V - E_0) - h\beta_h(V - E_0) \end{aligned} \quad (14)$$

where

$$\begin{aligned} \alpha_m(V) &= \frac{2.5 - 0.1V}{\exp(2.5 - 0.1V) - 1}, & \beta_m(V) &= 4 \exp\left(-\frac{V}{18}\right) \\ \alpha_n(V) &= \frac{0.1 - 0.01V}{\exp(1 - 0.1V) - 1}, & \beta_n(V) &= \frac{1}{8} \exp\left(-\frac{V}{80}\right) \\ \alpha_h(V) &= 0.07 \exp\left(-\frac{V}{20}\right), & \beta_h(V) &= \frac{1}{\exp(3 - 0.1V) + 1}. \end{aligned}$$

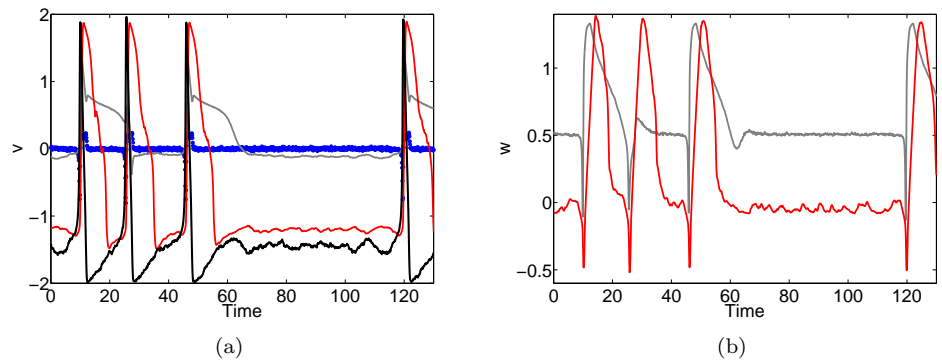


Fig 5. Results from assimilating extracellular Hodgkin-Huxley data (blue circles) to a Fitzhugh-Nagumo model. The scaled Hodgkin-Huxley intracellular potential (solid black line) is shown as a reference trajectory. Without bias correction (solid gray line), the filter is unable to reconcile the observational bias and as a result fails in estimating the system state. However, the bias-corrected filter (solid red line) is able to reconstruct the system dynamics.

The parameters of the Hodgkin-Huxley model are set to typical values: $C = 1, E_0 = -65, E_1 = 50, E_2 = -77, E_3 = -54.4$, and I_{noise} is a noisy current. Our observations of the Hodgkin-Huxley system consist of the extracellular potential approximated as

$$h(V, m, n, h) = -\frac{dV}{dt} = -\left(\frac{-g_1 m^3 h (V - E_1) - g_2 n^4 (V - E_2) - g_3 (V - E_3) + 7 + I_{\text{noise}}}{C}\right), \tag{15}$$

where 3000 ms of extracellular data sampled at rate $dt = 0.1$ are available. These observations are scaled to fit the bounds of the Fitzhugh-Nagumo model in order to prevent filter instability.

This example highlights several issues that are analogous to problems encountered in an experimental application. For starters, the model used by the data assimilation scheme (in our case the Fitzhugh-Nagumo equations) is often a simplified representation of the experimental system producing the spike data. This results in a degree of model error, or dynamical mismatch, which in effect leads to observational bias. Additionally, the frequency of the data spikes often do not match those of the assimilation model. To help account for this discrepancy prior to assimilation, we rescale the observation time of the data to help match the spiking frequency of the model to that of the data.

Fig. 5 shows the results from assimilating the extracellular Hodgkin-Huxley data (blue circles) using Eq. 9 with parameters $I = 0.5$ and $\tau = 14$. The scaled Hodgkin-Huxley voltage variable (solid black line) is shown in Fig. 5a as a reference trajectory. Without bias correction (solid gray line), the filter is unable to estimate an accurate representation of the intracellular dynamics. Using $d = 9$ delays and $N = 20$ neighbors to reconstruct the bias, the bias-corrected filter (solid red line) is able to converge to a reasonable estimate of the intracellular variables. Note that we are not able to perfectly reconstruct the Hodgkin-Huxley voltage; this is impossible due to the discrepancy between the dynamics of the Hodgkin-Huxley data and those of the Fitzhugh-Nagumo assimilation model.

Tracking in vivo intracellular potential

We now consider the reconstruction of experimental intracellular dynamics from recorded extracellular potential. The data analyzed were collected from an experiment [2] that performed simultaneous intracellular and extracellular recordings in the CA1 region of the hippocampus of anesthetized rats [1,3]. Fig. 6 shows example waveforms, scaled to match the bounds of the assimilation model, from typical intracellular (Fig. 6a) and extracellular (Fig. 6b) spikes in the dataset. Light blue traces represent individual waveforms and thick solid blue line represent the average waveform. These simultaneous recordings are difficult to make and are not typical of most experimental studies, where usually only the extracellular potential is measured. As such, we treat the intracellular data strictly as a mechanism for evaluation of our assimilation results.

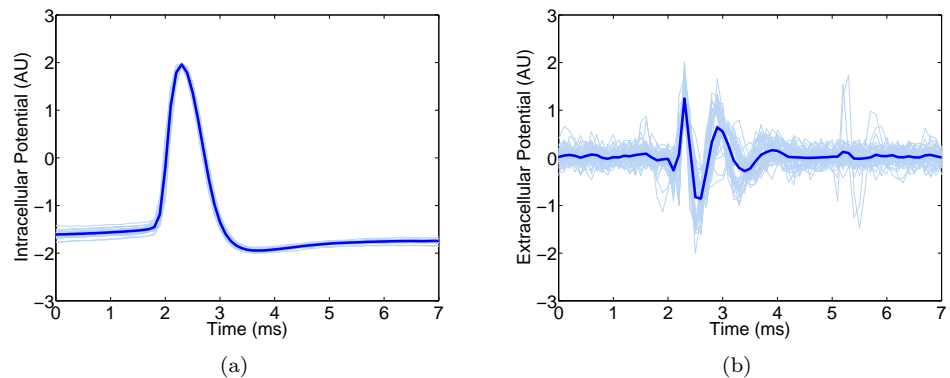


Fig 6. Representative waveforms (light blue traces) from recorded (a) intracellular and (b) extracellular spikes in the analyzed dataset. Dark blue lines denote the average detected waveform. Data are sampled at rate $dt = 0.01$ ms. While the authors in [1,3] collected simultaneous intracellular and extracellular measurements, experiments usually are centered around the extracellular recordings. We therefore treat the intracellular data as a mechanism for comparison purposes, and focus on the assimilation of the readily available extracellular measurements.

Our goal is to assimilate the readily available extracellular data, sampled at rate $dt = 0.01$, to the intracellular Fitzhugh-Nagumo model and reconstruct the appropriate intracellular dynamics. Note that the nature of extracellular recordings leads to measurements from several different cells, and thus in our assimilation of these observations we are in fact reconstructing the intracellular dynamics from several different neurons. Similarly to the Hodgkin-Huxley results, we don't expect a perfect reconstruction of the intracellular potential given the amount of discrepancy between the Fitzhugh-Nagumo system and the experimental data.

Fig. 7 shows the results of estimating the intracellular dynamics given the extracellular observations. The thin light lines represent the estimated dynamics corresponding to the individual extracellular spikes shown in Fig. 6b. The thick dark lines represent the average reconstructed dynamic. Without bias correction (Fig. 7a-b), the estimate of intracellular potential and recovery variable suffers. Using $d = 9$ delays and $N = 10$ neighbors for bias reconstruction, our bias corrected filter (Fig. 7c-d) is able to obtain an improved reconstruction of the intracellular dynamics. While the estimate is not perfect, which is to be expected since we are using an overly simplified assimilation model, we are still able to obtain a faithful representation of the intracellular potential and recovery variable.

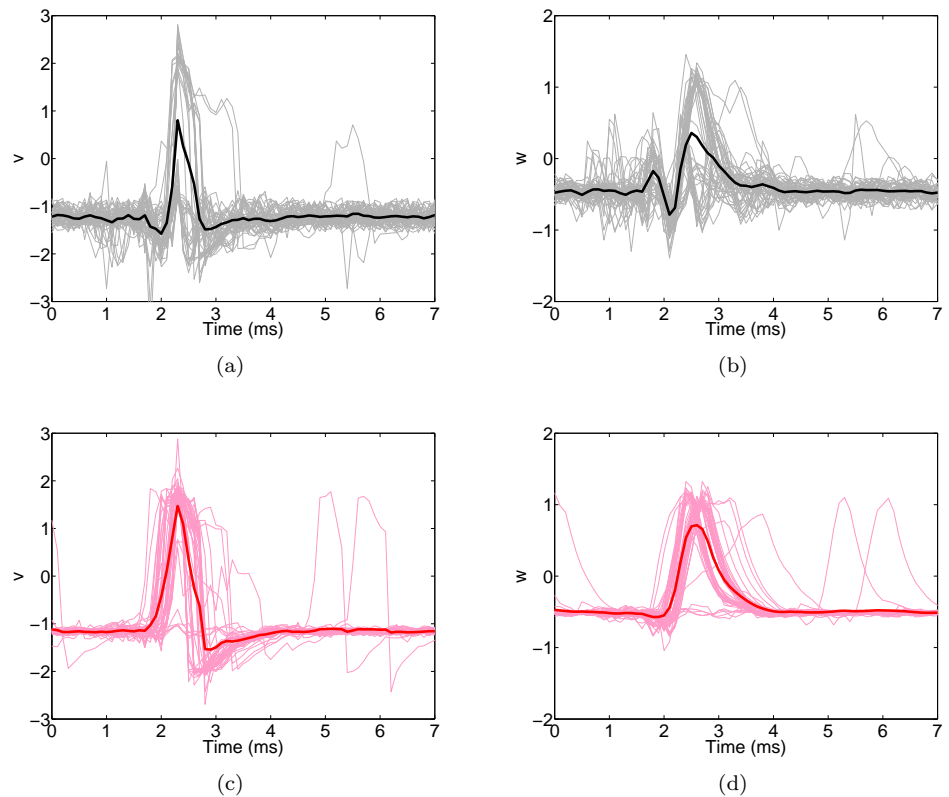


Fig 7. Results from assimilating the extracellular data to the Fitzhugh-Nagumo model. Thin light traces indicate individual events and thick dark line denotes the average waveform over the individual events. Estimated (a) intracellular potential and (b) recovery variable without bias correction results in an inaccurate reconstruction of the cell dynamics. With bias correction, we are able to learn the mapping from intracellular to extracellular state, and thus get an improved estimate of the intracellular potential and recovery dynamics, (c) and (d) respectively.

Conclusion

The successful implementation of data assimilation methods for estimation is dependent on an accurate mapping of the model state to the experimental measurements. This is done through application of an observation function. When this function is unknown or known with error, the observations are biased and the resulting state estimate suffers. The problem is exemplified in experimental neuroscience studies, where the relationship between extracellular potential observations and the corresponding intracellular state is complex. By leveraging a recent advance in data assimilation, we demonstrated the capability to learn this neuronal bias from available data, improving our ability to estimate intracellular neuronal state while reconciling severe model error resulting from dynamical mismatch.

As with most techniques that attempt to empirically learn a function, the resulting accuracy of the observation bias reconstruction is dependent on sufficient available data. In the neuroscience application examined here, enough spiking events must be available within the analyzed time series so that the extracellular-to-intracellular relationship can be approximated using the nearest-neighbors algorithm. Additionally, the use of any Kalman filter relies on Gaussian noise assumptions. For non-Gaussian noise processes,

more sophisticated data assimilation schemes may have to be considered. 246

The ability to accurately estimate the intracellular state from extracellular 247
measurements is a significant advantage in neuronal data analysis. While our focus here 248
is strictly on reconciling bias for state estimation, the problem can be further expanded 249
to include the estimation of physiological intracellular parameters. Future work will 250
examine this bias reconstruction problem in network-level neuroscience studies, where 251
the goal is an accurate estimation of network connectivity given extracellular 252
measurements. Finally, we believe that this technique will have wide-ranging 253
applicability to biological problems where the observation function may be known with 254
error. 255

References

1. Henze D, Borhegyi Z, Csicsvari J, Mamiya A, Harris K, Buzsáki G. Intracellular features predicted by extracellular recordings in the hippocampus in vivo. *Journal of Neurophysiology*. 2000;84:390–400.
2. Henze D, Harris K, Borhegyi Z, Csicsvari J, Mamiya A, Hirase H, et al.. Simultaneous intracellular and extracellular recordings from hippocampus region CA1 of anesthetized rats; 2009. CRCNS.org. <http://dx.doi.org/10.6080/K02Z13FP>.
3. Harris K, Henze D, Csicsvari J, Hirase H, Buzsáki G. Accuracy of tetrode spike separation as determined by simultaneous intracellular and extracellular measurements. *Journal of Neurophysiology*. 2000;84:401–414.
4. Hamilton F, Berry T, Peixoto N, Sauer T. Real-time tracking of neuronal network structure using data assimilation. *Physical Review E*. 2013;88:052715.
5. Hamilton F, Cressman J, Peixoto N, Sauer T. Reconstructing neural dynamics using data assimilation with multiple models. *Europhysics Letters*. 2014;107:68005.
6. Hamilton F, Berry T, Sauer T. Correcting observation model error in data assimilation; 2018. Preprint, <https://arxiv.org/abs/1803.06918>.
7. Kalman R. A new approach to linear filtering and prediction problems. *J Basic Eng*. 1960;82:35–45.
8. Simon D. *Optimal State Estimation: Kalman, H_∞ , and Nonlinear Approaches*. John Wiley and Sons; 2006.
9. Kalnay E. *Atmospheric modeling, data assimilation, and predictability*. Cambridge Univ. Press; 2003.
10. Evensen G. *Data assimilation: The Ensemble Kalman Filter*. Springer: Heidelberg; 2009.
11. Julier S, Uhlmann J, Durrant-Whyte H. A new method for the nonlinear transformation of means and covariances in filters and estimators. *IEEE Trans Automat Control*. 2000;45:477–482.
12. Julier S, Uhlmann J, Durrant-Whyte H. Unscented filtering and nonlinear estimation. *Proc IEEE*. 2004;92:401–422.

13. Rabier F. Overview of global data assimilation developments in numerical weather-prediction centres. *Quarterly Journal of the Royal Meteorological Society*. 2005;131(613):3215–3233.
14. Hunt BR, Kalnay E, Kostelich E, Ott E, Patil DJ, Sauer T, et al. Four-dimensional ensemble Kalman filtering. *Tellus A*. 2004;56(4):273–277.
15. Cummings JA. Operational multivariate ocean data assimilation. *Quarterly Journal of the Royal Meteorological Society*. 2005;131(613):3583–3604. doi:10.1256/qj.05.105.
16. Yoshida K, Yamaguchi J, Kaneda Y. Regeneration of Small Eddies by Data Assimilation in Turbulence. *Phys Rev Lett*. 2005;94:014501.
17. Law K, Stuart A. Evaluating data stimulation algorithms. *Mon Wea Rev*. 2012;140:3757–3782.
18. Schiff SJ. *Neural control engineering*. MIT Press; 2012.
19. Berry T, Sauer T. Adaptive ensemble Kalman filtering of nonlinear systems. *Tellus A*. 2013;65:20331.
20. Berry T, Harlim J. Correcting biased observation model error in data assimilation. *Monthly Weather Review*. 2017;145:2833–2853.
21. Takens F. Detecting strange attractors in turbulence. *Lecture Notes in Math* Springer-Verlag: Berlin. 1981;898.
22. Packard N, Crutchfield J, Farmer D, Shaw R. Geometry from a time series. *Phys Rev Lett*. 1980;45:712–715.
23. Sauer T, Yorke JA, Casdagli M. Embedology. *J Stat Phys*. 1991;65:579–616.
24. Sauer T. Reconstruction of shared nonlinear dynamics in a network. *Phys Rev Lett*. 2004;93:198701–4.
25. Fitzhugh R. Impulses and physiological states in theoretical models of nerve membrane. *Biophysical Journal*. 1961;1:445–466.
26. Nagumo J, Arimoto S, Yoshizawa S. An active pulse transmission line simulating nerve axon. *Proceedings of the IRE*. 1962;50:2061–2070.
27. Hodgkin A, Huxley A. A quantitative description of membrane current and its application to conduction and excitation in nerve. *J Physiology*. 1952;117:500–544.